International Journal of Control

Publication details, including instructions for authors and subscription information:
http://www.tandfonline.com/loi/tcon20

Integral sliding mode controller for precise manoeuvring of autonomous underwater vehicle in the presence of unknown environmental disturbances

Minsung Kim[a], Hangil Joe[b], Jinwhan Kim[c] & Son-cheol Yu[b]

[a] Future IT Innovation Laboratory, POSTECH, Pohang, Kyungbuk, Republic of Korea

[b] Department of Creative IT Engineering, POSTECH, Pohang, Kyungbuk, Republic of Korea

[c] Department of Mechanical Engineering, KAIST, Yuseong, Daejeon, Republic of Korea

Accepted author version posted online: 23 Mar 2015.Published online: 12 Jul 2015.

To cite this article: Minsung Kim, Hangil Joe, Jinwhan Kim & Son-cheol Yu (2015): Integral sliding mode controller for precise manoeuvring of autonomous underwater vehicle in the presence of unknown environmental disturbances, International Journal of Control, DOI: 10.1080/00207179.2015.1031182

To link to this article: http://dx.doi.org/10.1080/00207179.2015.1031182

International Journal of Control, 2015
http://dx.doi.org/10.1080/00207179.2015.1031182

Integral sliding mode controller for precise manoeuvring of autonomous underwater vehicle in the presence of unknown environmental disturbances

Minsung Kim[a], Hangil Joe[b], Jinwhan Kim[c] and Son-cheol Yu[b,*]

[a]*Future IT Innovation Laboratory, POSTECH, Pohang, Kyungbuk, Republic of Korea;* [b]*Department of Creative IT Engineering, POSTECH, Pohang, Kyungbuk, Republic of Korea;* [c]*Department of Mechanical Engineering, KAIST, Yuseong, Daejeon, Republic of Korea*

(*Received 16 July 2014; accepted 16 March 2015*)

We propose an integral sliding mode controller (ISMC) to stabilse an autonomous underwater vehicle (AUV) which is subject to modelling errors and often suffers from unknown environmental disturbances. The ISMC is effective in compensating for the uncertainties in the hydrodynamic and hydrostatic parameters of the vehicle and rejecting the unpredictable disturbance effects due to ocean waves, tides and currents. The ISMC is comprised of an equivalent controller and a switching controller to suppress the parameter uncertainties and external disturbances, and its closed-loop system is exponentially stable. Numerical simulations were performed to validate the proposed control approach, and experimental tests using Cyclops AUV were carried out to demonstrate its practical feasibility.

Keywords: robust controller; nonlinear systems; hydrodynamic uncertainties; hydrodynamic disturbances

1. Introduction

Autonomous underwater vehicles (AUVs) have been increasingly used for a variety of tasks in underwater environments including geological survey and data collection. For underwater surveys using AUVs, precise control is very important because the quality of data obtained is highly dependent on the vehicle's control performance in station keeping and/or trajectory tracking. However, the control of an AUV is difficult due to coupled nonlinearities, parameter uncertainties resulting from the lack knowledge of hydrodynamic coefficients and unknown external disturbances such as waves, tides, currents and upward or downward stream.

Considerable research has been conducted to address these problems, and various robust control strategies have been proposed to be used for an AUV in the literatures. A proportional-integral-derivative (PID) controller was applied to steering, diving and speed control of an AUV (Jarving, 1994). A decoupled proportional-derivative (PD) controller for AUVs using transformed equations of motion was described in Herman (2009); fast velocity reduction and the position error convergence were shown. Variable-structure PID control was also proposed to reduce the integral windup effect in Kim et al. (2013). The sliding mode controller (SMC) was first introduced to an AUV in Yoerger and Slotine (1985), and then the multivariable SMC was proposed separately for steering, diving and speed control of AUV in Healey and Lienard (1993). The second-order SMC was proposed for tracking control with reducing the chattering phenomenon in Bartolini and Punta (2000) and Joe et al. (2014). The output-feedback SMC was proposed for an underwater vehicle prototype by Pisano and Usai (2004); the second-order sliding mode differentiators were adopted to solve the output-feedback problems. Combining the SMC with fuzzy control technique, the sliding mode fuzzy control was developed for landing control of an AUV in Wang, Zhang, Hou, and Liang (2007). Since the output-feedback H_∞ controllers were developed for the linearised models of an AUV at different operating conditions in Silvestre and Pascoal (2004), the full-order H_∞ controller was applied to AUV in Feng and Allen (2010). H_∞ controllers for linear parameter varying polytopic systems and whose matrices are scheduled with regard to the varying control interval were presented in Roche et al. (2009, 2010). Recently, robust adaptive tracking controllers were used in Ismail and Dunnigan (2011) and Peng, Wang, and Hu (2011).

Among the aforementioned controllers, the SMC has attracted significant attention due to its simple structure and robustness to uncertain hydrodynamics and unknown disturbances. However, in practical systems, the standard SMC may suffer from high frequency oscillations due to the discontinuous switching control action. To decrease this high frequency oscillations, called a chattering phenomenon. A simple rule which makes the trajectory stay within a predetermined boundary layer was developed in Slotine (1984); continuous functions such as saturation functions, hyperbolic functions and hysteresis-saturation functions were used instead of discontinuous function in switching action in Park and Lee (1997).

* Corresponding author. Email: sncyu@postech.ac.kr

Another formulation for the sliding variable, based on the integral sliding mode concept, was introduced in Utkin and Shi (1996). The control scheme with this sliding variable is called the integral sliding mode controller (ISMC). ISMC does not have a reaching phase so that it ensures insensitivity of the trajectory with respect to uncertainties and disturbances from the initial stage. So far, a few researchers have employed ISMCs for AUV. Lea, Allen, and Merry (1999), Fu, Bian, Wang, and Gu (2005) and Tang, Zhou, Bian, and Jia (2010) showed performance improvements in transient response and carried out numerical simulations. But, in practical inspection tasks using AUV, station-keeping ability under uncertain hydrodynamics and unknown disturbances is a more important requirement for the control of AUV than the performance in the transient response. Therefore, we propose ISMC for an AUV and demonstrate the performance improvement in steady-state response under hydrodynamic uncertainties and unknown disturbances. The proposed controller consists of three components: 1) the linear controller keeps the closed-loop system within a uniform bound, 2) the nonlinear cancellation term cancels the nonlinear part of the AUV dynamics, and 3) the switching controller compensates for the steady-state error and suppresses the remaining bias term.

The proposed controller stabilises the AUV's motion in the presence of hydrodynamic uncertainties and unknown disturbances. Numerical simulations were performed to test the proposed ISMC in horizontal and vertical planes. Finally, experimental tests were conducted to demonstrate its practical feasibility.

This paper is organised as follows. In Section 2, the AUV modelling is derived. In Section 3, the proposed controller is presented and the stability of the closed-loop system is derived. In Section 4, experimental set-up is shown. Simulation and experimental results are presented in Section 5. Finally, conclusion is drawn in Section 6.

2. System modelling

2.1 AUV modelling

The motion of the AUV can be described using a body frame relative to a navigation frame (Figure 1). The AUV's linear velocities $[u\,v\,w]$ and angular velocities $[p\,q\,r]$ are described in the body frame, while the AUV's positions $[x\,y\,z]$ and orientation $[\phi\,\theta\,\psi]$ are described in the navigation frame. Since most open-frame vehicles are intrinsically stable in pitch and roll, we neglect roll and pitch motions and consider only horizontal and vertical motions corresponding to the linear velocities $[u\,v\,w]$, the angular velocity $[r]$, the position $[x\,y\,z]$ and the orientation $[\psi]$. The 4-degree of freedom (DOF) model was presented in Caccia and Veruggio (2000), and the hydrodynamics of the AUV is described as

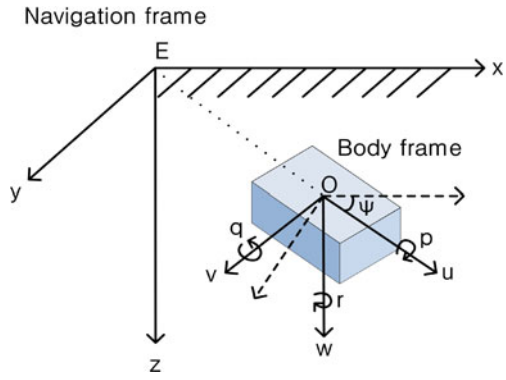

Figure 1. The navigation and body frames. Variables are defined in the text.

$$\mathbf{M}\dot{\mathbf{v}}(t)+\mathbf{C}(\mathbf{v}(t))\mathbf{v}(t)+\mathbf{D}(\mathbf{v}(t))\mathbf{v}(t)+\mathbf{g}(\boldsymbol{\eta}(t))=\mathbf{F}(t), \quad (1)$$

where

$$\mathbf{M}=\begin{bmatrix} m_u & 0 & 0 & 0\\ 0 & m_v & 0 & 0\\ 0 & 0 & m_w & 0\\ 0 & 0 & 0 & I_r \end{bmatrix},$$

$$\mathbf{C}(\mathbf{v}(t))=\begin{bmatrix} 0 & 0 & 0 & -m_v v(t)\\ 0 & 0 & 0 & m_u u(t)\\ 0 & 0 & 0 & 0\\ m_v v(t) & -m_u u(t) & 0 & 0 \end{bmatrix}, \quad (2)$$

$$\mathbf{D}(\mathbf{v}(t))=\begin{bmatrix} k_u+k_{u|u|}|u(t)| & 0 & 0 & 0\\ 0 & k_v+k_{v|v|}|v(t)| & 0 & 0\\ 0 & 0 & k_w+k_{w|w|}|w(t)| & 0\\ 0 & 0 & 0 & k_r+k_{r|r|}|r(t)| \end{bmatrix}, \quad (3)$$

$\mathbf{v}(t) = [u(t)\;\; v(t)\, w(t)\;\; r(t)]^T$, $\mathbf{g}(\boldsymbol{\eta}(t)) = [0\,0\,-W(t)\,0]^T$, $\mathbf{F}(t) = [F_u(t)\,F_v(t)\,F_w(t)\,T_r(t)]^T$; $u(t)$, $v(t)$ and $w(t)$ are the linear velocities in surge, sway and heave motions and $r(t)$ is the rotational velocity in yaw motion, m_u, m_v and m_w are the masses including hydrodynamic added masses in surge, sway and heave motions, I_r is the moment of inertia in yaw motion; $k_u/k_{u|u|}$, $k_v/k_{v|v|}$, $k_w/k_{w|w|}$ and $k_r/k_{r|r|}$ are uncertain linear/quadratic damping coefficients in surge, sway, heave and yaw motions, $F_u(t)$, $F_v(t)$ and $F_w(t)$ are the external forces acting on the vehicle in surge, sway and heave motions, $T_r(t)$ is the external torque acting on the vehicle in yaw motion, and $W(t)$ is buoyancy force in heave motion.

The kinematics of the AUV is described as

$$\dot{\boldsymbol{\eta}}(t) = \mathbf{J}(\boldsymbol{\eta}(t))\mathbf{v}(t), \tag{4}$$

where

$$\mathbf{J}(\boldsymbol{\eta}(t)) = \begin{bmatrix} \cos(\psi(t)) & -\sin(\psi(t)) & 0 & 0 \\ \sin(\psi(t)) & \cos(\psi(t)) & 0 & 0 \\ 0 & 0 & 1 & 0 \\ 0 & 0 & 0 & 1 \end{bmatrix} \tag{5}$$

and $\boldsymbol{\eta}(t) = [x(t)\, y(t)\, z(t)\, \psi(t)]^T$; $x(t)$, $y(t)$, $z(t)$ are the positions in surge, sway, and heave, respectively, and $\psi(t)$ is yaw angle.

The matrix including hydrostatic and hydrodynamic parameters satisfies the following properties.

(1) $\mathbf{M}$ is positive definite matrix i.e. $\mathbf{x}^{\mathbf{T}}(t)\mathbf{M}\mathbf{x}(t) > 0$, $\forall \mathbf{x}(t) \neq 0$.
(2) $\mathbf{C}(\mathbf{v}(t))$ is skew-symmetric matrix which is a square matrix whose transpose is its negative i.e. $\mathbf{C}(\mathbf{v}(t)) = -\mathbf{C}^{\mathbf{T}}(\mathbf{v}(t))$.
(3) $\mathbf{D}(\mathbf{v}(t))$ is positive definite matrix i.e. $\mathbf{x}^{\mathbf{T}}(t)\mathbf{D}(\mathbf{v}(t))\mathbf{x}(t) > 0$, $\forall \mathbf{x}(t) \neq 0$.
(4) $\mathbf{J}(\boldsymbol{\eta}(t))$ is non-singular matrix. Moreover, it satisfies $\mathbf{J}^{-\mathbf{1}}(\boldsymbol{\eta}(t)) = \mathbf{J}^{\mathbf{T}}(\boldsymbol{\eta}(t))$, $\dot{\mathbf{J}}(\boldsymbol{\eta}(t)) = \mathbf{J}(\boldsymbol{\eta}(t))\mathbf{S}(t)$ with skew-symmetric matrix

$$\mathbf{S}(t) = \begin{bmatrix} 0 & -\dot{\psi}(t) & 0 \\ \dot{\psi}(t) & 0 & 0 \\ 0 & 0 & 0 \end{bmatrix} = -\mathbf{S}^{\mathbf{T}}(t), \tag{6}$$

and $\dot{\mathbf{J}}^{-\mathbf{1}}(\boldsymbol{\eta}(t)) = \dot{\mathbf{J}}^{\mathbf{T}}(\boldsymbol{\eta}(t)) = \mathbf{S}^{\mathbf{T}}\mathbf{J}^{\mathbf{T}}(\boldsymbol{\eta}(t)) = -\mathbf{S}(t)\mathbf{J}(\boldsymbol{\eta}(t)) = -\mathbf{J}^{-\mathbf{1}}(\boldsymbol{\eta}(t))\mathbf{J}(\boldsymbol{\eta}(t))\mathbf{S}\mathbf{J}^{\mathbf{T}}(\boldsymbol{\eta}(t)) = -\mathbf{J}^{-\mathbf{1}}(\boldsymbol{\eta}(t))\dot{\mathbf{J}}(\boldsymbol{\eta}(t))\mathbf{J}^{-\mathbf{1}}(\boldsymbol{\eta}(t))$.

3. Controller design

Before we design ISMC, we first derive the second derivatives of $\boldsymbol{\eta}(t)$. Multiplying $\mathbf{J}^{-\mathbf{1}}(\boldsymbol{\eta}(t))$ and taking the derivative with respect to time on both sides of (4), we have

$$\begin{aligned} \dot{\mathbf{v}}(t) &= \dot{\mathbf{J}}^{-\mathbf{1}}(\boldsymbol{\eta}(t))\dot{\boldsymbol{\eta}}(t) + \mathbf{J}^{-\mathbf{1}}(\boldsymbol{\eta}(t))\ddot{\boldsymbol{\eta}}(t) \\ &= -\mathbf{J}^{-\mathbf{1}}(\boldsymbol{\eta}(t))\dot{\mathbf{J}}(\boldsymbol{\eta}(t))\mathbf{J}^{-\mathbf{1}}(\boldsymbol{\eta}(t))\dot{\boldsymbol{\eta}}(t) + \mathbf{J}^{-\mathbf{1}}(\boldsymbol{\eta}(t))\ddot{\boldsymbol{\eta}}(t). \end{aligned} \tag{7}$$

Substituting (7) into (1), we have

$$\begin{aligned} &\mathbf{M}\mathbf{J}^{-\mathbf{1}}(\boldsymbol{\eta}(t))\ddot{\boldsymbol{\eta}}(t) - \mathbf{M}\mathbf{J}^{-\mathbf{1}}(\boldsymbol{\eta}(t))\dot{\mathbf{J}}(\boldsymbol{\eta}(t))\mathbf{J}^{-\mathbf{1}}(\boldsymbol{\eta}(t))\dot{\boldsymbol{\eta}}(t) \\ &+ \mathbf{C}(\mathbf{v}(t))\mathbf{J}^{-\mathbf{1}}(\boldsymbol{\eta}(t))\dot{\boldsymbol{\eta}}(t) + \mathbf{D}(\mathbf{v}(t))\mathbf{J}^{-\mathbf{1}}(\boldsymbol{\eta}(t))\dot{\boldsymbol{\eta}}(t) + \mathbf{g}(\boldsymbol{\eta}(t)) \\ &= \mathbf{M}\mathbf{J}^{-\mathbf{1}}(\boldsymbol{\eta}(t))\ddot{\boldsymbol{\eta}}(t) + (\mathbf{C}(\mathbf{v}(t)) \\ &- \mathbf{M}\mathbf{J}^{-\mathbf{1}}(\boldsymbol{\eta}(t))\dot{\mathbf{J}}(\boldsymbol{\eta}(t)))\mathbf{J}^{-\mathbf{1}}(\boldsymbol{\eta}(t))\dot{\boldsymbol{\eta}}(t) \\ &+ \mathbf{D}(\mathbf{v}(t))\mathbf{J}^{-\mathbf{1}}(\boldsymbol{\eta}(t))\dot{\boldsymbol{\eta}}(t) + \mathbf{g}(\boldsymbol{\eta}(t)) = \mathbf{F}(t). \end{aligned} \tag{8}$$

Defining

$$\mathbf{M}_{\eta}(\boldsymbol{\eta}(t)) = \mathbf{M}\mathbf{J}^{-\mathbf{1}}(\boldsymbol{\eta}(t)), \tag{9}$$

$$\mathbf{C}_{\eta}(\mathbf{v}(t), \boldsymbol{\eta}(t)) = (\mathbf{C}(\mathbf{v}(t)) - \mathbf{M}\mathbf{J}^{-\mathbf{1}}(\boldsymbol{\eta}(t))\dot{\mathbf{J}}(\boldsymbol{\eta}(t)))\mathbf{J}^{-\mathbf{1}}(\boldsymbol{\eta}(t)), \tag{10}$$

$$\mathbf{D}_{\eta}(\mathbf{v}(t), \boldsymbol{\eta}(t)) = \mathbf{D}(\mathbf{v}(t))\mathbf{J}^{-\mathbf{1}}(\boldsymbol{\eta}(t)), \tag{11}$$

and considering hydrodynamic parameter uncertainties and unknown disturbances, we can rewrite (8) as

$$\begin{aligned} \ddot{\boldsymbol{\eta}}(t) = &-\mathbf{M}_{\eta}^{-\mathbf{1}}(\boldsymbol{\eta}(t))\mathbf{C}_{\eta}(\mathbf{v}(t), \boldsymbol{\eta}(t))\dot{\boldsymbol{\eta}}(t) \\ &- \mathbf{M}_{\eta}^{-\mathbf{1}}(\boldsymbol{\eta}(t))\mathbf{D}_{\eta}(\mathbf{v}(t), \boldsymbol{\eta}(t))\dot{\boldsymbol{\eta}}(t) \\ &+ \mathbf{M}_{\eta}^{-\mathbf{1}}(\boldsymbol{\eta}(t))\mathbf{F}(t) + \mathbf{H}(t), \end{aligned} \tag{12}$$

where $\mathbf{H}(t) = [H_1(t)\, H_2(t)\, H_3(t)\, H_4(t)]^T$ is the lumped uncertainty;

$$H_i(t) = \Delta H_i(\boldsymbol{\eta}(t), \dot{\boldsymbol{\eta}}(t), \mathbf{g}(\boldsymbol{\eta}(t)), \mathbf{d}(t)), \tag{13}$$

for all $i = 1, \ldots, 4$ where $\mathbf{d}(t)$ is unknown external disturbance. The lumped uncertainty $\mathbf{H}(t)$ fulfils the matching condition

$$\mathbf{H}(t) \in \text{span}(\mathbf{M}_{\eta}^{-\mathbf{1}}(\boldsymbol{\eta}(\mathbf{t}))). \tag{14}$$

The control objective is to design a feedback control law such that the positions of the AUV follow a given reference trajectory in the presence of uncertain hydrodynamics and unknown disturbances. The lumped uncertainty $\mathbf{H}(t)$, which includes uncertain hydrodynamics and unknown disturbances, can degrade the control performance and even cause the system to become unstable. To overcome this problem, we propose an ISMC for the AUV in the following section. The aim of ISMC is to constrain the AUV system to stay on a sliding surface $\mathbf{s}(t) = 0$, and thereby the error variable moves on the prescribed error dynamics.

3.1 Integral sliding mode controller

To help better understand ISMC, we start with choosing the sliding surface of the conventional SMC, which is well known for its robustness to hydrodynamic parameter uncertainties and external disturbances (Slotine & Li, 1991; Utkin, 1993). The conventional sliding surface is defined as

$$\mathbf{s}(t) = \dot{\mathbf{e}}(t) + \Lambda\mathbf{e}(t), \tag{15}$$

where $\mathbf{s}(t) = [s_1(t)\, s_2(t)\, s_3(t)\, s_4(t)]^T$, $\mathbf{e}(t) = \boldsymbol{\eta}_{\boldsymbol{r}}(t) - \boldsymbol{\eta}(t) = [e_1(t)\, e_2(t)\, e_3(t)\, e_4(t)]^T$ and $\boldsymbol{\Lambda} = \text{diag}(\lambda_1\, \lambda_2\, \lambda_3\, \lambda_4)$; $\boldsymbol{\eta}_{\boldsymbol{r}}(t) = [x_r(t)\, y_r(t)\, z_r(t)\, \psi_r(t)]^T$, λ_i is a positive constant for all $i = 1, \ldots, 4$; $x_r(t)$, $y_r(t)$, $z_r(t)$ and $\psi_r(t)$ are the reference positions in surge, sway, heave and yaw, respectively.

Besides the robustness against the hydrodynamic parameter uncertainties and unknown disturbances, ISMC improves steady-state accuracy by addressing the integral action to the conventional sliding surface (Khanh, Quang, That, Hong, & Ha, 2013). The integral augmented sliding surface is given as (Shi, Liu, & Bajcinca, 2008; Utkin & Shi, 1996)

$$\mathbf{s}(t) = \mathbf{K_p}\mathbf{e}(t) + \mathbf{K_i}\int_0^t \mathbf{e}(\tau)d\tau + \mathbf{K_d}\dot{\mathbf{e}}(t) - \mathbf{K_p}\mathbf{e}(0) - \mathbf{K_d}\dot{\mathbf{e}}(0), \quad (16)$$

where $\mathbf{K_p} = \text{diag}(k_{p1}\ k_{p2}\ k_{p3}\ k_{p4})$, $\mathbf{K_i} = \text{diag}(k_{i1}\ k_{i2}\ k_{i3}\ k_{i4})$, $\mathbf{K_d} = \text{diag}(k_{d1}\ k_{d2}\ k_{d3}\ k_{d4})$; k_{pi}, k_{ii} and k_{di} are positive constants, for all $i = 1, \ldots, 4$.

Because we choose the integral augmented sliding surface, we can determine the control law. To do that, we first take the derivative on both sides of (16) with respect to time. Then, we have

$$\dot{\mathbf{s}}(t) = \mathbf{K_p}\dot{\mathbf{e}}(t) + \mathbf{K_i}\mathbf{e}(t) + \mathbf{K_d}\ddot{\mathbf{e}}(t). \quad (17)$$

Substituting (12) into (17) yields

$$\begin{aligned}\dot{\mathbf{s}}(t) = {} & \mathbf{K_p}\dot{\mathbf{e}}(t) + \mathbf{K_i}\mathbf{e}(t) + \mathbf{K_d}(\ddot{\boldsymbol{\eta}}_r(t) \\ & + \mathbf{M}_\eta^{-1}(\boldsymbol{\eta}(t))\mathbf{C}_\eta(\mathbf{v}(t), \boldsymbol{\eta}(t))\dot{\boldsymbol{\eta}}(t) \\ & + \mathbf{M}_\eta^{-1}(\boldsymbol{\eta}(t))\mathbf{D}_\eta(\mathbf{v}(t), \boldsymbol{\eta}(t))\dot{\boldsymbol{\eta}}(t) \\ & - \mathbf{M}_\eta^{-1}(\boldsymbol{\eta}(t))\mathbf{F}(t) - \mathbf{H}(t)). \end{aligned} \quad (18)$$

Let the equivalent control law be

$$\begin{aligned}\mathbf{F_{eq}}(t) = {} & \mathbf{M}_\eta(\boldsymbol{\eta}(t))\mathbf{K_d^{-1}}(\mathbf{K_p}\dot{\mathbf{e}}(t) + \mathbf{K_i}\mathbf{e}(t)) \\ & + \mathbf{M}_\eta(\boldsymbol{\eta}(t))\ddot{\boldsymbol{\eta}}_r(t) + \mathbf{C}_\eta(\mathbf{v}(t), \boldsymbol{\eta}(t))\dot{\boldsymbol{\eta}}(t) \\ & + \mathbf{D}_\eta(\mathbf{v}(t), \boldsymbol{\eta}(t))\dot{\boldsymbol{\eta}}(t), \end{aligned} \quad (19)$$

where $\mathbf{K_p}$, $\mathbf{K_i}$ and $\mathbf{K_d}$ are chosen such that the polynomial $\mathbf{K_d}\ddot{\mathbf{e}}(t) + \mathbf{K_p}\dot{\mathbf{e}}(t) + \mathbf{K_i}\mathbf{e}(t)$ becomes a Hurwitz polynomial. Applying the control law (19) into (18) yields the resulting error dynamics

$$\begin{aligned}\dot{\mathbf{s}}(t) &= \mathbf{K_d}\ddot{\mathbf{e}}(t) + \mathbf{K_p}\dot{\mathbf{e}}(t) + \mathbf{K_i}\mathbf{e}(t) \\ &= -\mathbf{K_d}\mathbf{H}(t), \quad |(\mathbf{K_d}\mathbf{H}(t))_i| < \bar{H}_i, \end{aligned} \quad (20)$$

where $\bar{H}_i$ is the upper bound of the bias term $\mathbf{K_d}\mathbf{H}(t)$ for all $i = 1, \ldots, 4$. If the bias term becomes zero, we obtain the ideal error dynamics

$$\dot{\mathbf{s}}(t) = \mathbf{K_d}\ddot{\mathbf{e}}(t) + \mathbf{K_p}\dot{\mathbf{e}}(t) + \mathbf{K_i}\mathbf{e}(t) = 0. \quad (21)$$

However, $\mathbf{K_d}\mathbf{H}(t)$ prevents the tracking error $\mathbf{e}(t)$ from being zero. To suppress this bias term, we adopt the switching control input as (Slotine & Li, 1991)

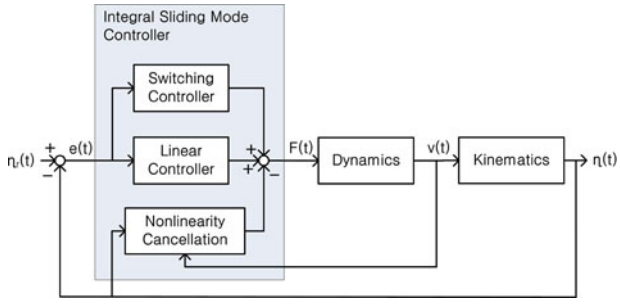

Figure 2. The schematic diagram of AUV control system.

$$\mathbf{F_{sw}}(t) = \mathbf{M}_\eta(\boldsymbol{\eta}(t))\mathbf{K_d^{-1}}\mathbf{K_{sw}}\mathbf{sgn}(\mathbf{s}(t)), \quad (22)$$

where $\mathbf{K_{sw}} = \text{diag}(k_{sw}\ k_{sw2}\ k_{sw3}\ k_{sw4})$, $\mathbf{sgn}(\mathbf{s}(t)) = [\text{sgn}(s_1(t))\ \text{sgn}(s_2(t))\ \text{sgn}(s_3(t))\ \text{sgn}(s_4(t))]^T$; k_{swi} is a positive constant, $k_{swi} \geq \bar{H}_i$ for all $i = 1, \ldots, 4$, and the signum function sgn(.) is defined as

$$\text{sgn}(x) \equiv \begin{cases} -1 & \text{if} \quad x < 0 \\ 0 & \text{if} \quad x = 0 \\ 1 & \text{if} \quad x > 0, \end{cases} \quad (23)$$

where x is a scalar variable.

Combining the equivalent and switching control laws yields the complete control law:

$$\begin{aligned}\mathbf{F_{eq}}(t) + \mathbf{F_{sw}}(t) = {} & \mathbf{M}_\eta(\boldsymbol{\eta}(t))\mathbf{K_d^{-1}}(\mathbf{K_p}\dot{\mathbf{e}}(t) + \mathbf{K_i}\mathbf{e}(t)) \\ & + \mathbf{M}_\eta(\boldsymbol{\eta}(t))\ddot{\boldsymbol{\eta}}_r(t) + \mathbf{C}_\eta(\mathbf{v}(t), \boldsymbol{\eta}(t))\dot{\boldsymbol{\eta}}(t) \\ & + \mathbf{D}_\eta(\mathbf{v}(t), \boldsymbol{\eta}(t))\dot{\boldsymbol{\eta}}(t) \\ & + \mathbf{M}_\eta(\boldsymbol{\eta}(t))\mathbf{K_d^{-1}}\mathbf{K_{sw}}\mathbf{sgn}(\mathbf{s}(t)). \end{aligned} \quad (24)$$

This control scheme (Figure 2) consists of three elements. The feedback term $\mathbf{M}_\eta(\boldsymbol{\eta}(t))\mathbf{K_d^{-1}}(\mathbf{K_p}\dot{\mathbf{e}}(t) + \mathbf{K_i}\mathbf{e}(t))$ makes the closed-loop system stable within a uniform error bound. The term $\mathbf{M}_\eta(\boldsymbol{\eta}(t))\ddot{\boldsymbol{\eta}}_r(t) + \mathbf{C}_\eta(\mathbf{v}(t), \boldsymbol{\eta}(t))\dot{\boldsymbol{\eta}}(t) + \mathbf{D}_\eta(\mathbf{v}(t), \boldsymbol{\eta}(t))\dot{\boldsymbol{\eta}}(t)$ compensates for the nonlinear part of the system. The switching input $\mathbf{M}_\eta(\boldsymbol{\eta}(t))\mathbf{K_d^{-1}}\mathbf{K_{sw}}\mathbf{sgn}(\mathbf{s}(t))$ suppresses the bias term $\mathbf{H}(t)$.

3.2 *Stability analysis*

To prove the stability of the closed-loop system, we choose the Lyapunov function candidate as

$$V(t) = \frac{1}{2}\mathbf{s}^T(t)\mathbf{s}(t). \quad (25)$$

Taking the derivative of the Lyapunov function candidate with respect to time, we have

$$\dot{V}(t) = \mathbf{s}^T(t)\dot{\mathbf{s}}(t). \quad (26)$$

Applying the control law (24) into (18) yields

$$\begin{aligned}\dot{\mathbf{s}}(t) &= -\mathbf{K_{sw}}\mathbf{sgn}(\mathbf{s}(t)) - \mathbf{K_d}\mathbf{H}(t)\\ &= \begin{bmatrix} -k_{sw1}\mathrm{sgn}(s_1(t)) - (\mathbf{K_d}\mathbf{H}(t))_1 \\ -k_{sw2}\mathrm{sgn}(s_2(t)) - (\mathbf{K_d}\mathbf{H}(t))_2 \\ -k_{sw3}\mathrm{sgn}(s_3(t)) - (\mathbf{K_d}\mathbf{H}(t))_3 \\ -k_{sw4}\mathrm{sgn}(s_4(t)) - (\mathbf{K_d}\mathbf{H}(t))_4 \end{bmatrix}. \end{aligned} \quad (27)$$

Substituting (27) into (26) yields

$$\begin{aligned}\dot{V}(t) &= \mathbf{s}^T(t)\dot{\mathbf{s}}(t)\\ &= s_1(t)(-k_{sw1}\mathrm{sgn}(s_1(t)) - (\mathbf{K_d}\mathbf{H}(t))_1)\\ &\quad + s_2(t)(-k_{sw2}\mathrm{sgn}(s_2(t)) - (\mathbf{K_d}\mathbf{H}(t))_2)\\ &\quad + s_3(t)(-k_{sw3}\mathrm{sgn}(s_3(t)) - (\mathbf{K_d}\mathbf{H}(t))_3)\\ &\quad + s_4(t)(-k_{sw4}\mathrm{sgn}(s_4(t)) - (\mathbf{K_d}\mathbf{H}(t))_4)\\ &= -k_{sw1}|s_1(t)| - s_1(t)(\mathbf{K_d}\mathbf{H}(t))_1\\ &\quad - k_{sw2}|s_2(t)| - s_2(t)(\mathbf{K_d}\mathbf{H}(t))_2\\ &\quad - k_{sw3}|s_3(t)| - s_3(t)(\mathbf{K_d}\mathbf{H}(t))_3\\ &\quad - k_{sw4}|s_4(t)| - s_4(t)(\mathbf{K_d}\mathbf{H}(t))_4\\ &\le -k_{sw1}|s_1(t)| + |s_1(t)|\bar{H}_1\\ &\quad - k_{sw2}|s_2(t)| + |s_2(t)|\bar{H}_2\\ &\quad - k_{sw3}|s_3(t)| + |s_3(t)|\bar{H}_3 - k_{sw4}|s_4(t)| + |s_4(t)|\bar{H}_4\\ &\le -|s_1(t)|(k_{sw1} - \bar{H}_1) - |s_2(t)|(k_{sw2} - \bar{H}_2)\\ &\quad - |s_3(t)|(k_{sw3} - \bar{H}_3) - |s_4(t)|(k_{sw4} - \bar{H}_4)\\ &\le -\lambda(|s_1(t)| + |s_2(t)| + |s_3(t)| + |s_4(t)|) \le -\lambda\sqrt{V}, \end{aligned} \quad (28)$$

where λ is the maximum value of $k_{swi} - \bar{H}_i$ for all $i = 1, \ldots, 4$. Therefore, the state trajectory reaches the surface $\mathbf{s}(t) = 0$ in a finite time T_f and remains there despite the bias term (Khalil & Grizzle, 2002). $\mathbf{s}(t) = 0$ means $\dot{\mathbf{s}}(t) = 0$ for all $t > T_f$. Because $\dot{\mathbf{s}}(t) = 0$, $\mathbf{e}(t)$ moves on the following error dynamics

$$\mathbf{K_d}\ddot{\mathbf{e}}(t) + \mathbf{K_p}\dot{\mathbf{e}}(t) + \mathbf{K_i}\mathbf{e}(t) = 0. \quad (29)$$

Because $\mathbf{K_p}$, $\mathbf{K_i}$ and $\mathbf{K_d}$ are chosen such that the polynomial $\mathbf{K_d}\ddot{\mathbf{e}}(t) + \mathbf{K_p}\dot{\mathbf{e}}(t) + \mathbf{K_i}\mathbf{e}(t)$ becomes a Hurwitz polynomial, $\mathbf{e}(t)$ is exponentially stable.

Remark 1: In the proposed controller scheme, the trajectory of AUV starts from the sliding surface $\mathbf{s}(0) = 0$ by the initial conditions in (16). Accordingly, the reaching phase is eliminated and robustness toward hydrodynamic uncertainties and unknown disturbances from the beginning is guaranteed.

Remark 2: The switching control action in (22) may cause the chattering due to delay and the imperfection of the switching device. The chattering results in wear-and-tear on the thrusters so that the system can be damaged in a short time. To reduce the chattering, we replace the signum function in (22) with a hyperbolic tangent function:

$$\mathbf{F_{sw}}(t) = \mathbf{M}_\eta(\boldsymbol{\eta}(t))\mathbf{K}_d^{-1}\mathbf{K_{sw}}\mathbf{tanh}(\Omega^{-1}\mathbf{s}(t)), \quad (30)$$

where $\mathbf{tanh}(\mathbf{\Omega^{-1}s}(t)) = [\tanh(\frac{s_1(t)}{\Omega_1})\tanh(\frac{s_2(t)}{\Omega_2})\tanh(\frac{s_3(t)}{\Omega_3}\tanh(\frac{s_4(t)}{\Omega_4})]^T$, $\mathbf{\Omega} = \mathrm{diag}(\Omega_1\ \Omega_2\ \Omega_3\ \Omega_4)$ denotes the thickness of boundary layer; Ω_1, Ω_2, Ω_3 and Ω_4 are positive constants.

Remark 3: In general, ISMC performs better than linear controller, because the signum function or hyperbolic tangent function gives larger control input responding to the same variation of error near the standard point where surface becomes zero. That is, ISMC works as high-gain controller around the point.

3.3 Force distribution

Because the number of thrusters is larger than the controllable DOF in the AUV, we need to distribute the control surface forces to the each thruster. To do that, we define the constraint optimisation problem as follows (Fossen, 1994):

$$\begin{aligned}&\min_{\mathbf{u}} J = \frac{1}{2}\mathbf{u}(t)^T\mathbf{W}\mathbf{u}(t)\\ &\text{subject to}\quad \mathbf{F}(t) = \mathbf{B}\mathbf{u}(t), \end{aligned} \quad (31)$$

where $\mathbf{W} = \mathbf{W^T}$ is the energy weighting matrix, $\mathbf{u}(t) = [u_{f1}(t)\ldots u_{f8}(t)]^T$ is the thruster force vector where u_{fi} is exerted force to the thruster u_i; subscript $i = 1, \ldots, 8$ represents the thruster, and $\mathbf{B}$ is the thruster force/torque distribution matrix. If $\mathbf{BW^{-1}B^T}$ is non-singular, one can easily show that

$$\mathbf{u}(t) = \mathbf{B}^\dagger\mathbf{F}(t), \quad (32)$$

where $\mathbf{B}^\dagger = \mathbf{W^{-1}B^T(BW^{-1}B^T)^{-1}}$. When all the thrusters are equally weighted, that is, $\mathbf{W} = \mathbf{I}$, the generalised inverse becomes $\mathbf{B}^\dagger = \mathbf{B^T(BB^T)^{-1}}$.

The thruster force/torque distribution matrix $\mathbf{B}$ is defined as

$$\mathbf{B} = \begin{bmatrix} 1 & 1 & 0 & 0 & 0 & 0 & 0 & 0 \\ 0 & 0 & 1 & 1 & -1 & -1 & 0 & 0 \\ 0 & 0 & 0 & 0 & 0 & 0 & 1 & 1 \\ 0 & 0 & d_c\sin(\theta_c) & -d_c\sin(\theta_c) & -d_c\sin(\theta_c) & d_c\sin(\theta_c) & 0 & 0 \end{bmatrix}, \quad (33)$$

where d_c is the distance from the centre of gravity of the AUV to the point where each thruster force acts, and θ_c is the angle between position and force vectors. The energy weighting matrix $\mathbf{W}$ is set to the identity matrix.

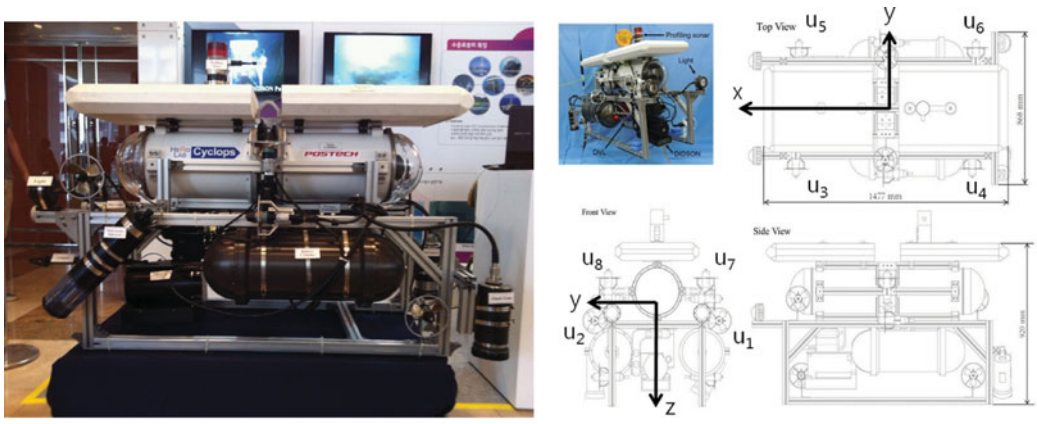

(a) (b)

Figure 3. The Cyclops underwater vehicle: (a) the side of Cyclops and (b) the structure of Cyclops.

4. Experimental set-up

To demonstrate the feasibility of the developed controller, it was applied to Cyclops (Figure 3 (a) and 3(b)), an AUV was developed at Hazardous Environmental Robotics Laboratory at the Pohang University of Science and Technology (POSTECH).

The AUV measures $1477 \times 868 \times 920$ mm (L × W × H) and weighs 219.8 kg. Two batteries are attached to the bottom of the AUV and a buoyancy sheet is attached to its top. A cylinder to contain the computer system is located in the centre of the AUV. As shown in Figure 3(b), this AUV is equipped with two thrusters (u_1, u_2) for surge motion, two thrusters (u_7, u_8) for heave motion, and four thrusters (u_3, u_4, u_5, u_6) for sway and yaw motion; the thrust range of the each thruster is from −50 to 50 N, a Doppler velocity log for measuring AUV positions and velocities, a fibre-optic gyro unit for measuring heading and yaw rate, and a digital pressure transducer for measuring the AUV's depth.

Cyclops (Table 1) includes an internal computer system. The internal computer system consists of two PC104 modules i.e. a main module and a submodule. Both modules use the Windows XP operating system. The main module functions as a control tower; this module receives the sensor data from submodule and sends the control signal to the thrusters. The PC104 submodule receives the sensor data and relays them to the main PC104 module. The developed controller was programmed using Visual Studio 2008 in the external computer system and downloaded to the main module in Cyclops. The controller runs at sampling interval $T = 100$ ms.

Table 1. The specification of Cyclops.

Specification	Value
Maximum speed	2 knots
Maximum operating time	2 h
Maximum operating depth	100 m
Actuators	8 thrusters with 475 W dc motors
Batteries	Two Li-Po (24V, 600W·h)
Computer system	Two PC104 modules (Pentium 4 1.4 GHz)
Sensors	Doppler velocity log (1.2 MHz), Fibre-optic gyroscope, Digital pressure transducer, Imaging sonar (1.1/1.8 MHz), Profiling sonar, Still camera and flash gun, Two pan-tilt cameras

Motion control test was conducted in the engineering basin in Korea Institute of Robotics and Convergence at POSTECH (Figure 4 (a) and 4(b)). The engineering basin is about $12 \times 8 \times 6$ m (L × W × H). The engineering basin is not equipped with a wave generator, so we cannot test the developed controller under the environment with the wave and current disturbances. In the engineering basin, the only applicable disturbance to the AUV is the buoyancy force. To produce the disturbance such as upward stream in the engineering basin environment, we applied the positive buoyancy of 2.5 N to the AUV of which the underwater weight was set to zero using a weight. Therefore, among surge, sway, yaw and heave motions, controller test in heave motion was conducted in the experiment.

5. Simulation and experimental results

5.1 Simulation result

To demonstrate the feasibility of the developed controller, we conducted various computer simulations with a model of the Cyclops AUV (Figure 3(a) and 3(b)). The controller parameters can be determined based on the parameter values of Cyclops (Table 2). Undetermined parameters are the gains of ISMC. A heuristic method was used to obtain these gains; the values obtained were $\lambda_i = 4$, $k_{swi} = 5$, $\Omega_i = 0.5$ for SMC, $k_{pi} = 4$, $k_{ii} = 4$, $k_{di} = 1$, $k_{swi} = 5$, $\Omega_i =$

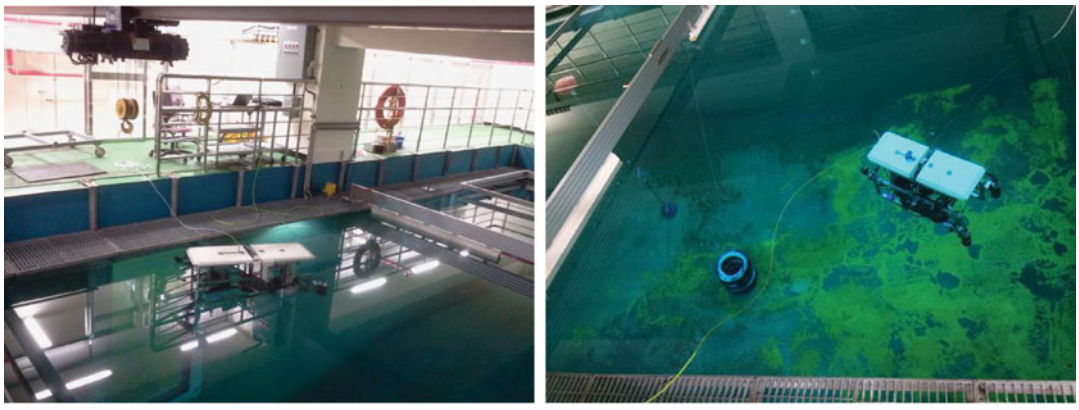

(a) (b)

Figure 4. Cyclops in the engineering basin.

0.5 for ISMC for all $i = 1, \ldots, 3$, $\lambda_4 = 1$, $k_{sw4} = 1$, $\Omega_4 = 0.5$ for SMC and $k_{p4} = 1$, $k_{i4} = 0.5$, $k_{d4} = 1$, $k_{sw4} = 0.5$, $\Omega_4 = 0.5$ for ISMC. We varied the linear/quadratic drag coefficients by ±20% from their true values for AUV model. We added the sinusoidal disturbances (e.g. waves) with 10 N amplitude, 0.13 Hz frequency and constant disturbances (e.g. currents) with 1 N to surge and sway motions, uniformly distributed random signals with 10 N amplitude to surge, sway and heave motions, and constant disturbance (e.g. buoyancy) with 5 N amplitude to heave motion. Finally, we set the sampling period to 100 ms and simulated this control scheme for 20 s in horizontal motion for 150 s in vertical motion using Matlab software.

Under the above setting, and ramp input commands in surge and sway as $x_r(t) = 0.1t$ m and $y_r(t) = 0.01t$ m, and $\psi_r(t) = 0$, we first tested PD plus nonlinear cancellation (NC), SMC and ISMC in horizontal motion.

Table 2. The parameter values of Cyclops.

Cyclops parameter	Value
Weight of Cyclops in air m	219.8 kg
Weight of Cyclops underwater $\bar{m}$	0 kg
Length of Cyclops l	1477 mm
Width of Cyclops w	868 mm
Height of Cyclops h	920 mm
Distance from the centre of gravity d_c	580 mm
Angle between position and force vectors θ_c	115.5°
Mass of Cyclops in surge m_u	391.5 kg
Linear drag coefficient in surge k_u	16
Quadratic drag coefficient in surge $k_{u\|u\|}$	229.4
Mass of Cyclops in sway m_v	639.6 kg
Linear drag coefficient in sway k_v	131.8
Quadratic drag coefficient in sway $k_{v\|v\|}$	328.3
Mass of Cyclops in heave m_w	639.6 kg
Linear drag coefficient in heave k_w	65.6
Quadratic drag coefficient in heave $k_{w\|w\|}$	296.8
Buoyancy force in heave $W(t)$	2.5 N

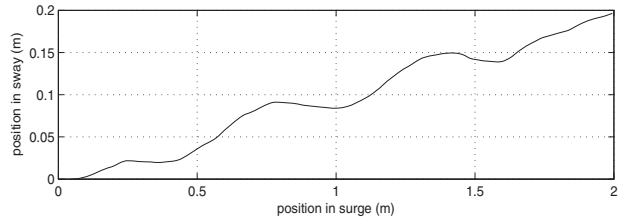

Figure 5. Command input response in surge, sway and yaw when PD plus nonlinear cancellation is applied.

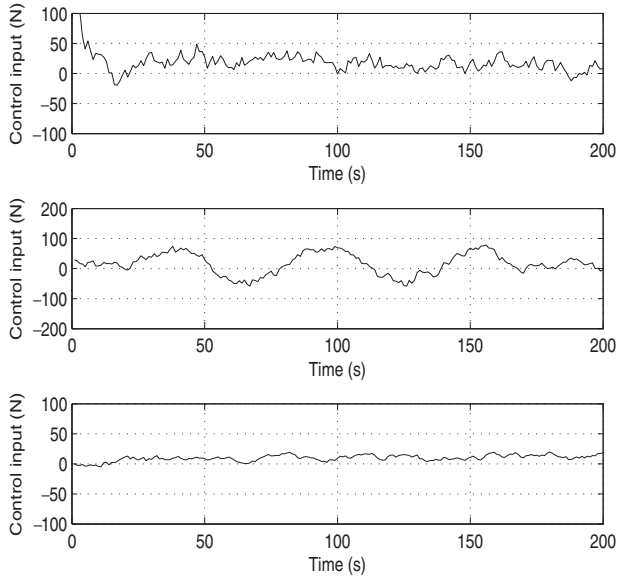

Figure 6. Controller input in surge (top), sway (middle) and yaw (bottom) when PD plus nonlinear cancellation is applied.

PD plus nonlinear cancellation worked poorly (Figure 5) because PD controller cannot suppress the sinusoidal disturbance. However, SMC and ISMC worked well, because the switching controller can suppress the sinusoidal

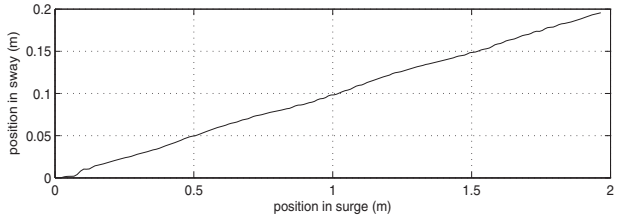

Figure 7. Command input response in surge, sway and yaw when SMC is applied.

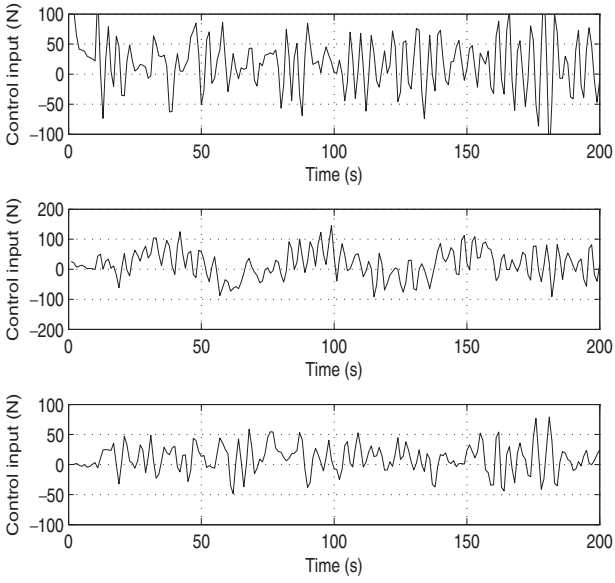

Figure 8. Controller input in surge (top), sway (middle) and yaw (bottom) when SMC is applied.

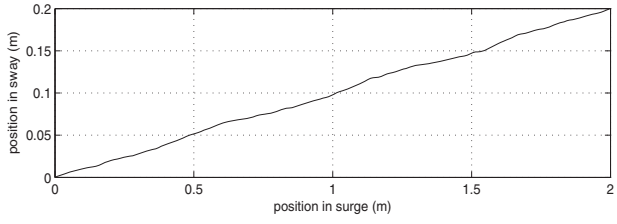

Figure 9. Command input response in surge, sway and yaw when ISMC is applied.

disturbance. However, it still has a steady-state error such that the position of Cyclops in horizontal plane cannot reach the end point (2, 0.15) (Figure 7). With ISMC, the sinusoidal disturbance is well suppressed, and the steady-state error does not exist (Figure 9). The control inputs are shown in Figures 6, 8 and 10.

In heave motion test, we applied these controllers with step input command ($z_r(t) = 0.1$ m), and sinusoidal input command

$$z_r(t) = \frac{1}{20} - \frac{1}{20}\cos\left(\frac{2\pi t}{100}\right). \tag{34}$$

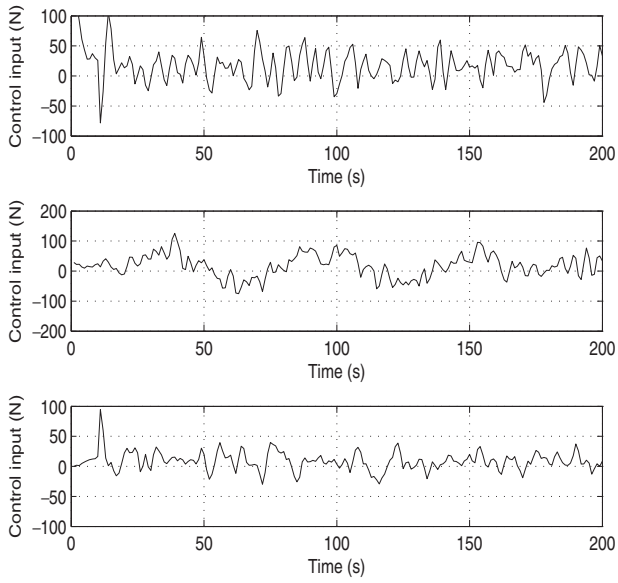

Figure 10. Controller input in surge (top), sway (middle) and yaw (bottom) when ISMC is applied.

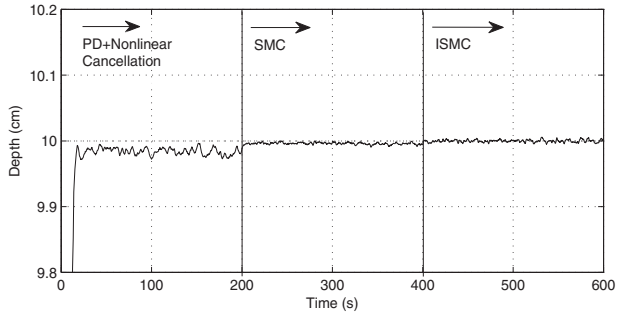

Figure 11. Step input response in heave.

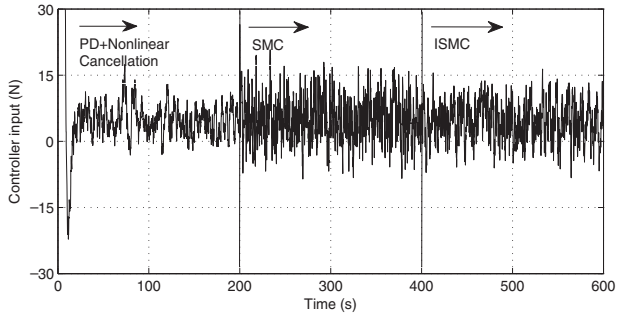

Figure 12. Control input in heave when the step input command is applied.

PD plus nonlinear cancellation and SMC have a small steady-state error due to the buoyancy force, but it can be eliminated when ISMC is used (Figures 11). The control inputs are shown in Figures 12 and 14.

To show the accuracy and effort of the proposed controller quantitatively, and 13 we examined the root-mean-square (rms) errors of the command input responses in

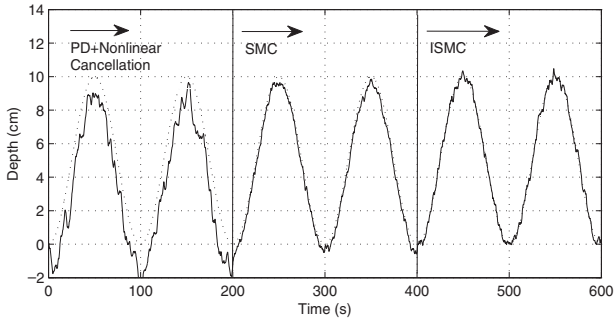

Figure 13. Sinusoidal input response in heave.

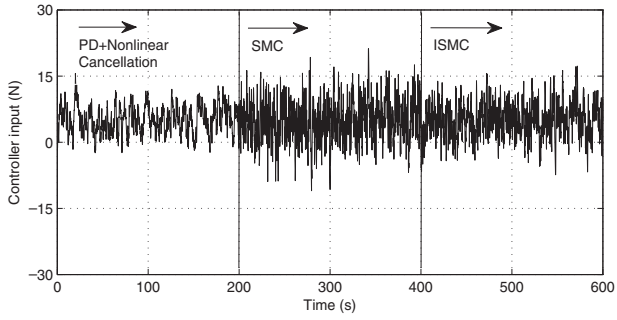

Figure 14. Control input in heave when the sinusoidal input command is applied.

Table 3. Rms errors in surge, sway and yaw at steady state.

Controller	Surge (m)	Sway (m)	Yaw (m)
PD plus NC	8.7×10^{-2}	1.0×10^{-2}	6.0×10^{-2}
SMC	3.5×10^{-2}	4.4×10^{-3}	6.9×10^{-3}
ISMC	9.1×10^{-3}	2.2×10^{-3}	1.1×10^{-2}

Table 4. Rms errors in heave at steady state.

Controller	Heave with step input (cm)	Heave with sinusoidal input (cm)
PD plus NC	5.5×10^{-2}	1.6×10^{-2}
SMC	4.2×10^{-3}	4.1×10^{-3}
ISMC	2.0×10^{-3}	2.0×10^{-3}

surge, sway and yaw (Table 3), and heave (Table 4) and the rms control inputs in surge, sway and yaw (Table 5), and heave (Table 6). ISMC shows smaller rms error than PD plus nonlinear cancellation and SMC, and smaller rms control input in steady-state than SMC.

5.2 *Experimental result*

To demonstrate the effectiveness of proposed controller, we investigate the regulation and trajectory tracking problems in experiments using Cyclops AUV. The control parameters were determined based on actual measurements (Table 2).

Table 5. Rms control inputs in surge, sway and yaw at steady state.

Controller	Surge (N)	Sway (N)	Yaw (N)
PD plus NC	2.4×10	3.7×10	1.3×10
SMC	3.9×10	5.3×10	2.9×10
ISMC	3.2×10	4.0×10	1.9×10

Table 6. Rms control inputs at steady state.

Controller	Heave with step input (N)	Heave with sinusoidal input (N)
PD plus NC	5.9×10	6.4×10
SMC	6.8×10	6.7×10
ISMC	6.4×10	6.4×10

Undetermined parameters are the gains of ISMC. A heuristic method was used to obtain these gains; the values obtained were $\lambda_4 = 1$, $k_{sw4} = 1$, $\Omega_4 = 0.5$ for SMC, $k_{p4} = 1$, $k_{i4} = 0.5$, $k_{d4} = 1$, $k_{sw4} = 0.5$, $\Omega_4 = 0.5$ for ISMC with step input command, $\lambda_4 = 1$, $k_{sw4} = 1$, $\Omega_4 = 0.5$ for SMC and $k_{p4} = 1$, $k_{i4} = 0.5$, $k_{d4} = 1$, $k_{sw4} = 0.5$, $\Omega_4 = 0.5$ for ISMC with sinusoidal input command.

Under the above parameter setting, we first applied the proposed controller to Cyclops AUV with step input command ($z_r(t) = 1$ m). We applied PD plus nonlinear cancellation for the first 50 s, and applied SMC from 50 to 100 s. Afterward, we applied ISMC. PD plus nonlinear cancellation could not compensate for the constant disturbance such as buoyancy force. SMC also could not compensate for the constant disturbance, because the delay elements in digital implementation and sensor decreased the tracking performance of SMC. Although ISMC also experienced the system delay, it could compensate for the disturbance relatively well owing to the integral term defined on the sliding surface, thereby reducing the steady-state error in heave (Figure 15). A hyperbolic tangent function was used to the switching inputs of both SMC and ISMC to reduce the damage on the thrusters. This hyperbolic tangent function caused the switching control input of SMC to vary widely.

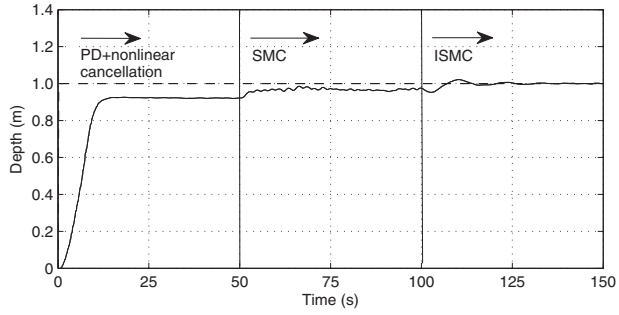

Figure 15. Step input response in heave.

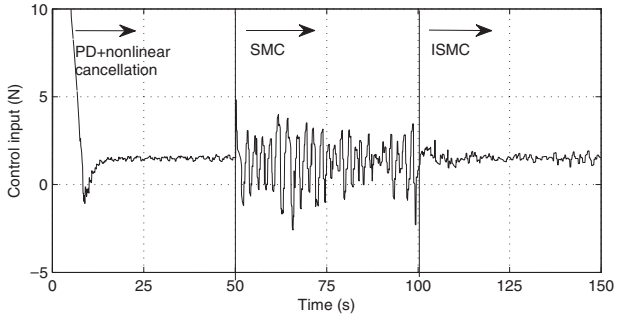

Figure 16. Control input in heave when the step input command is applied.

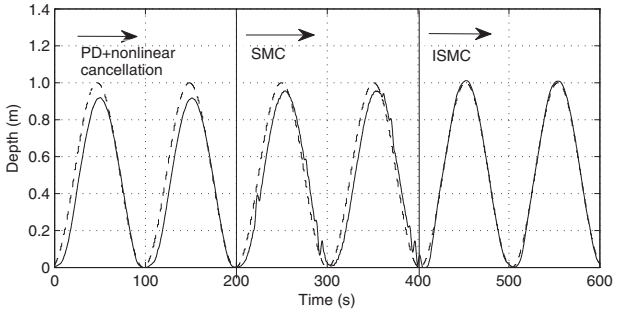

Figure 17. Sinusoidal input response in heave.

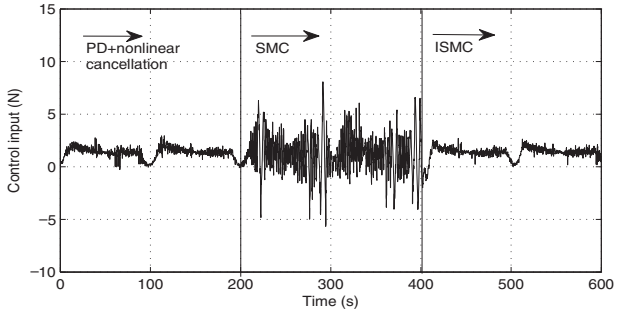

Figure 18. Control input in heave when the sinusoidal input command is applied.

Conversely, the switching control input of ISMC varied within a relatively narrow range due to the offset produced by the integral term defined on the sliding surface. The resulting control inputs are represented in Figure 16. To test the tracking performance of the closed-loop system with proposed controller, we applied it to Cyclops AUV with sinusoidal input as

$$z_r(t) = \frac{1}{2} - \frac{1}{2}\cos\left(\frac{2\pi t}{100}\right). \tag{35}$$

We also applied PD plus nonlinear cancellation for the first 200 s, and applied SMC from 200 to 400 s. Afterward, we applied ISMC. Similar to the results in the regulation problem, the position of Cyclops tracked the sinusoidal input command in heave only when ISMC was applied (Figure 17). Variations of control inputs are also shown in Figure 18 .

6. Conclusion

In this paper, we propose an ISMC for an AUV. The ISMC compensates for uncertain hydrodynamics and compensates for disturbances such as waves, tides, currents and upward or downward stream. The proposed controller guarantees that the closed-loop system is exponentially stable under parameter uncertainties and unknown disturbances. We tested the proposed controller in surge, sway and heave using a computer simulation of an AUV model and in heave using a real AUV. Comparison of the accuracy of PD plus nonlinear cancellation, SMC and ISMC in the simulation and experimental results verify that the proposed controller increases the accuracy of trajectory tracking for AUV in the presence of uncertain hydrodynamics and unknown disturbances.

Disclosure statement

No potential conflict of interest was reported by the authors.

Funding

This research was supported by the MSIP (Ministry of Science, ICT and Future Planning), Korea, under the "ICT Consilience Creative Program" (IITP-2015-R0346-15-1007) supervised by the IITP (Institute for Information & communications Technology Promotion); this research was a part of the project titled "Gyeongbuk Sea Grant Program", funded by the Ministry of Oceans and Fisheries, Korea and partly supported by the Civil Military Technology Cooperation Center, Korea.

References

Bartolini, G., & Punta, E. (2000). Second order sliding mode tracking control of underwater vehicles. *American Control Conference, 1*(6), 65–69.

Caccia, M., & Veruggio, G. (2000). Guidance and control of a reconfigurable unmanned underwater vehicle. *Control Engineering Practice, 8*(1), 21–37.

Feng, Z.P., & Allen, R. (2010). H_∞ autopilot design for autonomous underwater vehicles. *Journal of Shanghai Jiaotong University (Science), 15*(2), 194–198.

Fossen, T.I. (1994). *Guidance and control of ocean vehicles* (Vol. 199, No. 4). New York, NY: Wiley.

Fu, M., Bian, X., Wang, W., & Gu, J. (2005, July). Research on sliding mode controller with an integral applied to the motion of underwater vehicle. In *IEEE International Conference on Mechatronics and Automation* (pp. 2144–2149), Niagara Falls.

Healey, A.J., & Lienard, D. (1993). Multivariable sliding mode control for autonomous diving and steering of unmanned underwater vehicles. *IEEE Journal of Oceanic Engineering, 18*(3), 327–339.

Herman, P. (2009). Decoupled PD set-point controller for underwater vehicles. *Ocean Engineering, 36*(6), 529–534.

Ismail, Z.H., & Dunnigan, M.W. (2011). Tracking control scheme for an underwater vehicle-manipulator system with single and multiple sub-regions and sub-task objectives. *IET Control Theory and Applications, 5*(5), 721–735.

Jarving, B. (1994). The NDRE-AUV flight control system. *IEEE Journal of Oceanic Engineering, 19*(4), 497–501.

Joe, H., Kim, M. & Yu, S.C. (2014). Second-order sliding-mode controller for autonomous underwater vehicle in the presence of unknown disturbances. *Nonlinear Dynamics, 78*(1), 183–196.

Khalil, H.K., & Grizzle, J.W. (2002). *Nonlinear systems* (Vol. 3). Upper Saddle River, NJ: Prentice hall.

Khanh, Q.N., Quang, V.D., That, N.D., Hong, Q.N., & Ha, Q.P. (2013, November). Observer-based integral sliding mode control for sensorless PMSM drives using FPGA. In *2013 International Conference on Control, Automation and Information Sciences (ICCAIS)* (pp. 218–223), Nha Trang.

Kim, M., Joe, H., Pyo, J., Kim, J., Kim, H., & Yu, S.C. (2013, September). Variable-structure PID controller with Anti-windup for Autonomous underwater vehicle. In *OCEANS-San diego* (pp. 1–5). MTS/IEEE.

Lea, R.K., Allen, R., & Merry, S.L. (1999). A comparative study of control techniques for an underwater flight vehicle. *International Journal of Systems Science, 30*(9), 947–964.

Park, K.B., & Lee, J.J. (1997). Sliding mode controller with filtered signal for robot manipulators using virtual plant/controller. *Mechatronics, 7*(3), 277–286.

Peng, Z., Wang, D., & Hu, X. (2011). Robust adaptive formation control of underactuated autonomous surface vehicles with uncertain dynamics. *IET Control Theory and Applications, 5*(12), 1378–1387.

Pisano, A., & Usai, E. (2004). Output-feedback control of an underwater vehicle prototype by higher-order sliding modes. *Automatica, 40*(9), 1525–1531.

Roche, E., Sename, O., & Simon, D. (2009, August). LPV/H_∞ control of an autonomous underwater vehicle (AUV). In *Proceedings of the European Control Conference* (pp. 3160–3165), Budapest.

Roche, E., Sename, O., & Simon, D. (2010). LFT/H_∞ varying sampling control for Autonomous Underwater Vehicles. In *Proceedings of 4th IFAC Symposium on System, Structure and Control*, Ancona, Italy.

Shi, J., Liu, H., & Bajcinca, N. (2008). Robust control of robotic manipulators based on integral sliding mode. *International Journal of Control, 81*(10), 1537–1548.

Silvestre, C., & Pascoal, A. (2004). Control of the INFANTE AUV using gain scheduled static output feedback. *Control Engineering Practice, 12*(12), 1501–1509.

Slotine, J.J.E. (1984). Sliding controller design for non-linear systems. *International Journal of Control, 40*(2), 421–434.

Slotine, J.J.E., & Li, W. (1991). *Applied nonlinear control*. New Jersey: Prentice hall.

Tang, Z., Zhou, J., Bian, X., & Jia, H. (2010). Simulation of optimal integral sliding mode controller for the depth control of auv. In *IEEE International Conference on Information and Automation (ICIA)* (pp. 2379–2383), Harbin.

Utkin, V.I. (1993). Sliding mode control design principles and applications to electric drives. *IEEE Transactions on Industrial Electronics, 40*(1), 23–36.

Utkin, V., & Shi, J. (1996, December). Integral sliding mode in systems operating under uncertainty conditions. In *Proceedings of the 35th IEEE on Decision and Control* (pp. 4591–4596), Kobe.

Wang, S., Zhang, H., Hou, W., & Liang, J. (2007). Control and navigation of the variable buoyancy AUV for underwater landing and takeoff. *International Journal of Control, 80*(7), 1018–1026.

Yoerger, D., & Slotine, J. (1985). Robust trajectory control of underwater vehicles. *IEEE Journal of Oceanic Engineering, 10*(4), 462–470.